20/11/2024 08:11

(Article begins on next page)

Effect of a rigid toroidal inhomogeneity on the elastic properties of a composite

Stanislav Krasnitskii
Petra Velikogo Institut fiziki nanotehnologij i telekommunikacij, Sankt-Peterburgskij politehniceskij universitet, St Petersburg, Russia

Anton Trofimov
Center for Design, Manufacturing and Materials, Skolkovo Institute of Science and Technology, Skolkovo, Russia

Enrico Radi
Department of Science and Methods in Engineering, University of Modena and Reggio Emilia, Modena, Italy

Igor Sevestianov
Department of Mechanical and Aerospace Engineering, New Mexico State University, Las Cruces, NM, USA

Abstract
An analytical solution is obtained for the problem of an infinite elastic medium containing a rigid toroidal inhomogeneity under remotely applied uniform strain. The traction on the torus surface is determined as a function of torus parameters and strain components applied at infinity. The results are utilized to calculate components of the stiffness contribution tensor of the rigid toroidal inhomogeneity that is required for calculation of the overall elastic properties of a material containing multiple toroidal inhomogeneities. The analytical results are verified by comparison with finite element model calculations.

1. Introduction

The paper focuses on the problem of a rigid inhomogeneity of toroidal shape embedded in an elastic matrix. Inhomogeneities of this kind occur in both natural and man-made materials. Figure 1 provides several examples. Barium titanate nanotori are used as nonvolatile memory devices, transducers, optical modulators, sensors, and more recently possible energy storage in supercapacitors [1]. Toroidal particles

---

Corresponding author:
Igor Sevostianov, Department of Mechanical and Aerospace Engineering, New Mexico State University, Las Cruces, NM, USA.
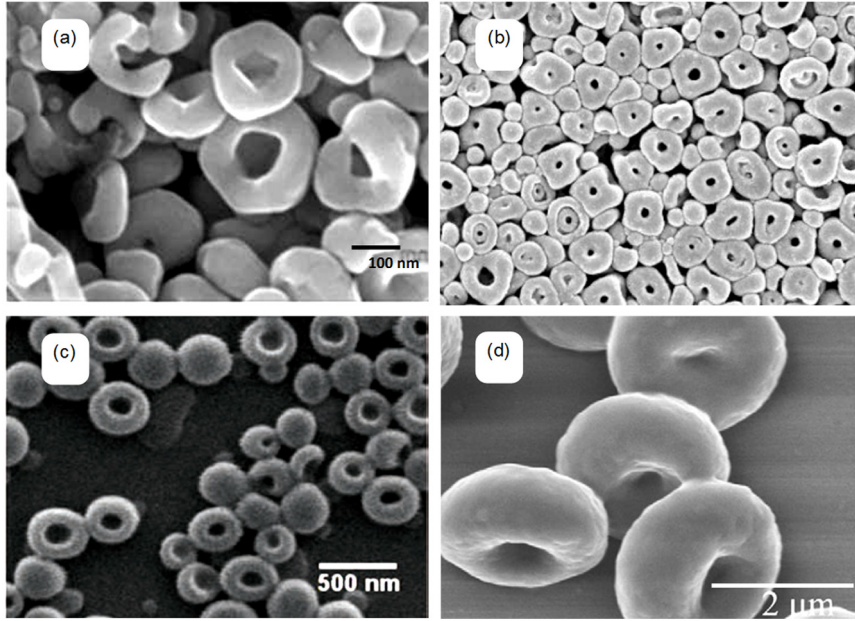Email: igor@nmsu.edu

Figure 1. (a) The morphology of BaTiO3 nanotorus [1]; (b) copolymer bilayer toroidal vesicles have the potential application in biomimicry [7]; (c), (d) polymeric toroidal particles [8], [9]

represent the preferred morphology of Li_2O_2 deposition on porous carbon electrodes in lithium–oxygen batteries [2,3]. Polymeric "microdonuts" are used in bioengineering [4]. The toroidal shape of nanoparticles is reported to be preferred for microwave absorption properties of $BaTiO_3$ [5]. Onaka et al. [6] reported the formation of toroidal particles of SiO_2 in a Cu matrix due to internal oxidation of a Cu–Si solid-solution polycrystal. Analytical modeling of materials with such microstructure has not been well developed. In the homogenization schemes, the inhomogeneities are usually assumed to be of ellipsoidal shape. This unrealistic assumption is largely responsible for insufficient linkage between methods of micromechanics and materials science applications.

While many analytical and numerical results have been obtained for two-dimensional non-elliptical inhomogeneities [10–13], only a limited number of numerical results and approximate estimates are available for non-ellipsoidal three-dimensional (3D) shapes. Most of them are related to pores and cracks. In the context of compliance of irregularly shaped cracks, certain results have been obtained [14–18]. Various concave pores have also been analyzed [19–22].

For toroidal shapes, Argatov and Sevostianov [23] used asymptotic methods to evaluate the contribution of a thin rigid toroidal inhomogeneity into overall stiffness. Onaka and colleagues [6,24,25] derived analytical expressions for components of the Eshelby tensor for a toroidal inclusion. We emphasize, however, that the Eshelby tensor for non-ellipsoidal inhomogeneities is irrelevant to the problem of effective properties of a heterogeneous material (as clearly seen from the formulation of the two Eshelby problems; see, for example, Chen et al. [21]). The problem on the effective conductivity (thermal or electric) of a material containing toroidal insulating inhomogeneities has been addressed by Radi and Sevostianov [26].

The present work focuses on the evaluation of the contribution provided by a rigid toroidal inhomogeneity to effective elastic properties. We first consider a homogeneous elastic material (matrix), with the stiffness tensor $\mathbf{C}^0$ assumed to be isotropic. It contains an inhomogeneity, of volume $V^{(1)}$, of a different elastic material with the compliance and stiffness tensor $\mathbf{C}^1$. The contribution of the inhomogeneity to the overall stress, per representative volume V (the extra stress, as compared to the homogeneous matrix) is given by the fourth-rank tensor $\mathbf{N}$– the stiffness contribution tensor of the inhomogeneity – defined by

$$\Delta\boldsymbol{\sigma} = \frac{V^{(1)}}{V}\mathbf{N} : \boldsymbol{\varepsilon}^{\infty} \tag{1}$$

where ε^{∞} is the "remotely applied" strain. For a rigid inhomogeneity, this additional stress field $\Delta\boldsymbol{\sigma}$ can be represented as integral over the inhomogeneity boundary [27]

$$\Delta\boldsymbol{\sigma} = \frac{1}{V}\int_S (\boldsymbol{\sigma}\cdot\boldsymbol{n})\otimes\boldsymbol{x}\,dA, \tag{2}$$

where $\boldsymbol{n}$ is the outward unit normal to the inhomogeneity surface S at point $\boldsymbol{x}$.

To calculate components of the stiffness contribution tensor of a rigid toroidal inhomogeneity, a displacement boundary value problem has to be solved for 3D elastic space containing such and inhomogeneity. This problem has been addressed previously [28–30]. In the text to follow, we modify the previous solution to calculate the components of the stiffness contribution tensor.

2. Formulation of the problem in toroidal coordinates

We consider a rigid circular torus embedded in an infinite elastic medium subject to remotely applied homogeneous strain field. Following Morse and Feshbach [31] and Lebedev and Silverman [32], we introduce a toroidal coordinate system (α,β,φ) (Figure 2) defined by the following relations

$$x = \frac{c\,\sinh\alpha\,\cos\varphi}{\cosh\alpha - \cos\beta}, y = \frac{c\,\sinh\alpha\,\sin\varphi}{\cosh\alpha - \cos\beta}, z = \frac{c\,\sin\beta}{\cosh\alpha - \cos\beta}. \tag{3}$$

where c denotes the distance of the poles from the origin, $\alpha > 0$, $\beta \in [-\pi, \pi]$, and $\varphi \in [0, 2\pi]$.

Constant values of the bipolar coordinate α describe a family of toroidal surfaces. R_0 and r_0 denote medium radius of the torus and the radius of its circular cross-section, respectively. Then

$$\alpha_0 = \cosh^{-1}(R_0, r_0), c = r_0\,\sinh\,\alpha_0 = \sqrt{R_0^2 - r_0^2}. \tag{4}$$
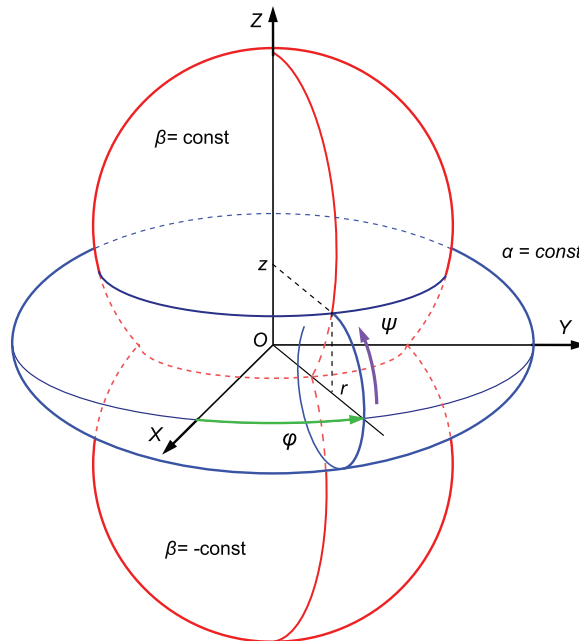
Figure 2. Toroidal coordinate system (α, β, φ). Associated Cartesian (*x, y, z*) and cylindrical (*r, φ, z*) coordinate systems are also shown. The coordinate surfaces α_0 = const are the eccentric family of tori and $\beta_0 = \pm$const are spherical caps having there centers along the z-axis. ψ is the so-called poloidal angel of the torus ring.

With reference to an arbitrary meridian section, the poloidal angle $\psi \in [-\pi, \pi]$ around the circle defined by a constant value of α is associated with the toroidal coordinate β by the following relations:

$$\sin \psi = \frac{\sinh \alpha \sin \beta}{\cosh \alpha - \cos \beta} \quad \text{and} \quad \cos \psi = \frac{\cosh \alpha \cos \beta - 1}{\cosh \alpha - \cos \beta}. \tag{5}$$

Then a torus surface $\alpha = \alpha_0$ can be defined parametrically as follows:

$$x = (R_0 + r_0 \cos \psi) \cos \varphi, \, y = (R_0 + r_0 \cos \psi) \sin \varphi, \, z = r_0 \sin \psi. \tag{6}$$

Let

$$P^k_{n-1/2}(\cosh \alpha) = \frac{\Gamma(n + 1/2 + k)}{\pi \, \Gamma(n + 1/2)} \int_0^\pi (\cosh \alpha + \sinh \alpha \, \cos t)^{n-1/2} \cos kt \, dt, \tag{7}$$

$$Q^k_{n-1/2}(\cosh \alpha) = \frac{(-1)^k}{2\sqrt{2\pi}} \Gamma(k + 1/2) \sinh^k \alpha \int_{-\pi}^{\pi} \frac{\cos nt}{(\cosh \alpha - \cos t)^{k+1/2}} \, dt, \tag{8}$$

denote the associated Legendre function of semi-integer index and order k of the first or the second kind, respectively [32–34]. They satisfy the following equations

$$\Delta_k \, P^k_{n-1/2}(\cosh \alpha) = 0, \, \Delta_k \, Q^k_{n-1/2}(\cosh \alpha) = 0, \tag{9}$$

where the operator Δ_k is defined by

$$\Delta_k = \frac{\partial^2}{\partial r^2} + \frac{1}{r}\frac{\partial}{\partial r} + \frac{\partial^2}{\partial z^2} - \frac{k}{r^2}. \tag{10}$$

3. Analytical solution for a rigid toroidal inclusion in an infinite elastic medium

The total displacement field $\mathbf{u}$ in the infinite elastic medium containing a rigid toroidal inclusion can be represented as a sum $\mathbf{u} = \mathbf{u}^\infty + \mathbf{u}^0$ where $\mathbf{u}^\infty$ corresponds to the remotely applied homogeneous strain field and $\mathbf{u}^0$ is the correction due to the presence of the toroidal inhomogeneity. Due to the geometrical symmetry of the problem, the stiffness contribution tensor $\mathbf{N}$ is expected to be transversely isotropic. Therefore, it is sufficient to consider the following Cartesian components of the remotely applied strains: ε^∞_{zz}, ε^∞_{yy}, and ε^∞_{yz}. Then, the fundamental displacement field admits the following Cartesian components

$$\begin{aligned} u^\infty_x &= 0 \\ u^\infty_y &= \varepsilon^\infty_{yy} y \\ u^\infty_z &= 2\varepsilon^\infty_{yz} y + \varepsilon^\infty_{zz} z \end{aligned} \tag{11}$$

The corresponding displacement components in cylindrical coordinates can be written as

$$\begin{aligned} u^\infty_r &= \frac{1}{2}\varepsilon^\infty_{yy} r - \frac{1}{2}\varepsilon^\infty_{yy} r \cos 2\varphi \\ u^\infty_\phi &= \frac{1}{2}\varepsilon^\infty_{yy} r \sin 2\varphi \\ u^\infty_z &= \varepsilon^\infty_{zz} z + 2\varepsilon^\infty_{yz} r \sin \varphi \end{aligned} \tag{12}$$

For the general case of arbitrary load, the inhomogeneity may be subjected to rigid body translation and rotation. In this case the boundary conditions on the inhomogeneity surface could be represented in the form of the Robin problem [34] as $\mathbf{u} = \mathbf{d} + \boldsymbol{\omega} \times \mathbf{x}$, where $\mathbf{d}$ and $\boldsymbol{\omega}$ are vectors of small translation and rotation of the rigid inhomogeneity, and $\mathbf{x}$ is a position vector on the interface. In the case of tensile strain $\varepsilon_{zz}^{\infty}$ and $\varepsilon_{yy}^{\infty}$, the rigid motion of the torus can be ignored due to the symmetry of the applied loads and geometry. In contrast, simple shear deformation $\varepsilon_{yz}^{\infty}$ leads to the rigid rotation of the toroid with respect to its center with $\mathbf{d} = 0$ and $\boldsymbol{\omega} = \omega \, \mathbf{e_x}$, where ω is the rotation angle of the torus (to be determined) and $\mathbf{e_x}$ is a unit vector along the x-axis. Then, in the cylindrical coordinate system,

$$u_r = -\omega z \sin \varphi$$

$$u_\varphi = -\omega z \cos \varphi$$

$$u_z = \omega r \sin \varphi \tag{13}$$

In the study by Krokhmal [35], it was suggested to seek for the corrective term $\mathbf{u}^0$ in the following form

$$u_r^0 = \frac{1}{2} u_0^0(\alpha, \beta) + u_2^0(\alpha, \beta) \cos 2\varphi$$

$$u_\varphi^0 = v_2^0(\alpha, \beta) \sin 2\varphi$$

$$u_z^0 = \frac{1}{2} w_0^0(\alpha, \beta) + w_1^0(\alpha, \beta) \sin \varphi \tag{14}$$

where

$$u_0^0 = \phi_1 + \gamma r \vartheta_0, \quad w_0^0 = \chi_0 + \gamma z \vartheta_0, \quad w_1^0 = \chi_1 + \gamma z \vartheta_1$$
$$u_2^0 = \phi_3 + \psi_1 + \gamma r \vartheta_2, \quad v_2^0 = \phi_3 - \psi_1 \tag{15}$$

$\gamma = 1/[4(1-\nu)]$, and the functions ϑ_k, ϕ_k, ψ_k, and χ_k satisfy the following relations

$$\Delta_k \vartheta_k = 0, \Delta_{k+1} \phi_{k+1} = 0, \Delta_{k-1} \psi_{k-1} = 0, \Delta_k \chi_k = 0, \tag{16}$$

and the differential constraint

$$\gamma \left(1 + \frac{1}{\gamma} + r \frac{\partial}{\partial r} + z \frac{\partial}{\partial z} \right) \vartheta_k + \left(\frac{\partial}{\partial r} + \frac{k+1}{r} \right) \phi_{k+1} + \left(\frac{\partial}{\partial r} - \frac{k-1}{r} \right) \psi_{k-1} + \frac{\partial}{\partial z} \chi_k = 0, (k \ge 0) \tag{17}$$

with $\psi_{-1} = 0$.

The general solutions to equations (16) matching the displacement field of equations (12) and (13) have the following form

$$\vartheta_k = \frac{1}{c} \sqrt{\cosh \alpha - \cos \beta} \sum_{n=0}^{+\infty}{}' A_{n,k} P_{n-1/2}^k (\cosh \alpha) \cos (n\beta - k^2 \pi/2)$$

$$\phi_k = \sqrt{\cosh \alpha - \cos \beta} \sum_{n=0}^{+\infty}{}' B_{n,k} P_{n-1/2}^{k+1} (\cosh \alpha) \cos (n\beta - k^2 \pi/2)$$

$$\psi_k = \sqrt{\cosh \alpha - \cos \beta} \sum_{n=0}^{+\infty}{}' D_{n,k} P_{n-1/2}^{k-1} (\cosh \alpha) \cos (n\beta - k^2 \pi/2)$$

$$\chi_k = \sqrt{\cosh\alpha - \cos\beta} \sum_{n=0}^{+\infty}{}' C_{n,k} P_{n-1/2}^k(\cosh\alpha) \sin(n\beta - k^2\pi/2) \tag{18}$$

for $k = 0, 1, 2, 3$. The primed summation in equation (18) denotes that the first term of the sum corresponding to $n = 0$ is halved.

The unknown coefficients $A_{n,k}$, $B_{n,k}$, $C_{n,k}$, and $D_{n,k}$ can be determined from the boundary condition at $\alpha = \alpha_0$, together with the differential constraint (equation (17)). By using equations (11)–(14), the boundary conditions at $\alpha = \alpha_0$ require

$$u_0^0(\alpha_0,\beta) = -\varepsilon_{yy}^\infty r|_{\alpha=\alpha_0} \quad u_1^0(\alpha_0,\beta) = -\omega z|_{\alpha=\alpha_0} \quad u_2^0(\alpha_0,\beta) = \frac{1}{2}\varepsilon_{yy}^\infty r|_{\alpha=\alpha_0}$$

$$v_1^0(\alpha_0,\beta) = \omega z|_{\alpha=\alpha_0} \quad v_2(\alpha_0,\beta) = -\frac{1}{2}\varepsilon_{yy}^\infty r|_{\alpha=\alpha_0}$$

$$w_0^0(\alpha_0,\beta) = -2\varepsilon_{zz}^\infty z|_{\alpha=\alpha_0} \quad w_1^0(\alpha_0,\beta) = (\omega - 2\varepsilon_{yz}^\infty) r|_{\alpha=\alpha_0} \tag{19}$$

Introducing the unknowns $x_{n,k}$ for the coefficients $B_{n,k}$ and using equations (15) and (19), all the coefficients in the Fourier series of equation (18) can be written in terms of $x_{n,k}$ as follows

$$A_{0,k} = \varkappa_{0,k}(2x_{1,k} - 2\cosh\alpha_0 x_{0,k} + p_{0,k})/\gamma,$$

$$A_{n,k} = \varkappa_{n,k}(x_{n+1,k} - 2\cosh\alpha_0 x_{n,k} + x_{n-1,k} + p_{n,k})/\gamma, (n \geq 1)$$

$$B_{n,k} = \lambda_{n,k} x_{n,k}, (n \geq 0)$$

$$C_{0,0} = 0,$$

$$C_{0,1} = \varkappa_{0,1}(s_{0,1} - 2x_{1,1}),$$

$$C_{n,k} = \varkappa_{n,k}(x_{n-1,k} - x_{n+1,k} + s_{n,k}), (n \geq 1)$$

$$D_{n,k} = \gamma_{n,k}(x_{n,k} + q_{n,k}), (n \geq 0) \tag{20}$$

where

$$\varkappa_{n,k} = \frac{\delta_k}{\sinh\alpha_0 \, P_{n-1/2}^k(\cosh\alpha_0)}, \, \gamma_{n,k} = \frac{\varepsilon_k}{P_{n-1/2}^{k-1}(\cosh\alpha_0)}, \, \lambda_{n,k} = \frac{1}{P_{n-1/2}^{k+1}(\cosh\alpha_0)}, \tag{21}$$

being $\delta_0 = 1/2$, $\varepsilon_0 = 0$, and $\delta_k = \varepsilon_k = 1$, for $k \geq 1$. Coefficients $p_{n,k}$, $q_{n,k}$, and $s_{n,k}$ are the Fourier coefficients for the following functions

$$\sqrt{\cosh\alpha_0 - \cos\beta}\,(u_k^0 + \varepsilon_k v_k^0) = \delta_k \sum_{n=0}^{+\infty}{}' p_{n,k} \cos(n\beta - k^2\pi/2),$$

$$-\frac{\varepsilon_k v_k^0}{\sqrt{\cosh\alpha_0 - \cos\beta}} = \varepsilon_k \sum_{n=0}^{+\infty}{}' q_{n,k} \cos(n\beta - k^2\pi/2), \tag{22}$$

$$\frac{w_k^0 \sinh\alpha_0 - (u_k^0 + \varepsilon_k v_k^0)\,\sin\beta}{\sqrt{\cosh\alpha_0 - \cos\beta}} = \delta_k \sum_{n=0}^{+\infty}{}' s_{n,k} \sin(n\beta - k^2\pi/2),$$

Using the decomposition given in the Appendix, we finally obtain the following relations

$$p_{n,0} = -\frac{4\sqrt{2}}{\pi}\varepsilon_{yy}^\infty c \sinh\alpha_0 \, Q_{n-1/2}(\cosh\alpha_0)$$

$$q_{n,1} = 0$$

$$s_{n,0} = \frac{8\sqrt{2}}{\pi}(\varepsilon_{yy}^{\infty} - 2\varepsilon_{zz}^{\infty})c \sinh \alpha_0 \, n \, Q_{n-1/2}(\cosh \alpha_0)$$

$$p_{n,1} = 0$$

$$q_{n,1} = -\frac{4\sqrt{2}}{\pi}\omega c n \, Q_{n-1/2}(\cosh \alpha_0)$$

$$s_{n,1} = \frac{4\sqrt{2}}{\pi}(\omega - 2\varepsilon_{yz}^{\infty})c \sinh \alpha_0 \, Q_{n-1/2}^1(\cosh \alpha_0) \qquad (23)$$

$$p_{n,2} = 0$$

$$q_{n,2} = -\frac{2\sqrt{2}}{\pi}\varepsilon_{yy}^{\infty}c \sinh \alpha_0 \, Q_{n-1/2}^1(\cosh \alpha_0)$$

$$s_{n,2} = 0$$

and obtain the following infinite system of algebraic equations for the unknown variables $x_{n,k}$:

$$a_{n,k}x_{n+1,k} - b_{n,k}x_{n,k} + c_{n,k}x_{n-1,k} = d_{n,k}, \qquad (24)$$

where

$$a_{n,k} = -2(n+k+\delta_n)\varkappa_{n+1,k}\cosh \alpha_0 + (2n+1+2/\gamma)\varkappa_{n,k} - (n+k+1/2)(n+k+3/2)\lambda_{n+1,k} - \gamma_{n+1,k},$$

$$b_{n,k} = -2(n+k+1/2)\varkappa_{n+1,k} + 2\delta_n(1+2/\gamma)\varkappa_{n,k}\cosh \alpha_0 + 2\varepsilon_n(n-k-1/2)\varkappa_{n-1,k}$$
$$\quad - 2(n+k+1/2)(n-k-1/2)\lambda_{n,k} - 2\delta_n\gamma_{n,k},$$

$$c_{n,k} = \varepsilon_n[2(n-k-1/2)\varkappa_{n-1,k}\cosh \alpha_0 - (2n-1-2/\gamma)\varkappa_{n,k} - (n-k-1/2)(n-k-3/2)\lambda_{n-1,k} - \gamma_{n-1,k}],$$

$$d_{n,k} = \gamma_{n+1,k} \, q_{n+1,k} - 2\delta_n\gamma_{n,k} \, q_{n,k} + \varepsilon_n\gamma_{n-1,k} \, q_{n-1,k} - (n+k+1/2)\varkappa_{n+1,k}(p_{n+1,k}+s_{n+1,k})$$
$$\quad - \delta_n(1+2/\gamma)\varkappa_{n,k} \, p_{n,k} + \varepsilon_n(n-k-1/2)\varkappa_{n-1,k}(p_{n-1,k}-s_{n-1,k}) + \varepsilon_n \, 2n \, \varkappa_{n,k}s_{n,k}, \qquad (25)$$

for $n \geq 0$. Note that for $k = 0, 2$ equation (25) holds for $n \geq 0$, while for $k = 1$ it holds for $n \geq 1$.

A necessary condition for the series in equation (18) to be convergent is that the coefficients $A_{n,k}$, $B_{n,k}$, $C_{n,k}$ and $D_{n,k}$ tend to zero as $n \to \infty$. Thus, the unknown coefficients $x_{n,k}$ have to converge to zero. In this case, the infinite system of equations (24) can be solved explicitly using the procedure for tridiagonal matrix

$$x_n = \sum_{m=n}^{+\infty} \eta_{m+1} \prod_{k=n+1}^{m} \xi_k \qquad (26)$$

where

$$\xi_{n+1} = \frac{a_n}{b_n - c_n\xi_n}, \quad \eta_{n+1} = \frac{c_n\eta_n - d_n}{b_n - c_n\xi_n}.$$

From the conditions for $n = 0$ and $k = 0, 2$

$$\xi_1 = \frac{a_0}{b_0}, \quad \eta_1 = -\frac{d_0}{b_0}.$$

From the conditions for $n = 0$ and $k = 1$

$$\xi_1 = 0, \quad \eta_1 = 0.$$

Once the unknown coefficients $x_{n,k}$ have been determined, the total displacement field in cylindrical coordinates is given by the sum of equations (12), (13), and (14). Then, the corresponding strain field can be calculated from the compatibility condition:

$$\varepsilon_{rr} = \frac{\partial u_r}{\partial r}, \qquad\qquad \varepsilon_{\varphi\varphi} = \frac{1}{r}\frac{\partial u_\varphi}{\partial \varphi} + \frac{u_r}{r}, \qquad \varepsilon_{zz} = \frac{\partial u_z}{\partial z},$$
$$\varepsilon_{r\varphi} = \frac{1}{2}\left(\frac{1}{r}\frac{\partial u_r}{\partial \varphi} + \frac{\partial u_\varphi}{\partial r} - \frac{u_\varphi}{r}\right), \quad \varepsilon_{rz} = \frac{1}{2}\left(\frac{\partial u_r}{\partial z} + \frac{\partial u_z}{\partial r}\right), \quad \varepsilon_{\varphi z} = \frac{1}{2}\left(\frac{1}{r}\frac{\partial u_z}{\partial \varphi} + \frac{\partial u_\varphi}{\partial z}\right),$$

(27)

where we used connection between derivatives in cylindrical and toroidal coordinate systems

$$\frac{\partial}{\partial r} = \frac{1}{c}\left[(\cosh\alpha\cos\beta - 1)\frac{\partial}{\partial\alpha} + \sinh\alpha\sin\beta\frac{\partial}{\partial\beta}\right],$$

$$\frac{\partial}{\partial z} = \frac{1}{c}\left[-\sinh\alpha\sin\beta\frac{\partial}{\partial\alpha} + (\cosh\alpha\cos\beta - 1)\frac{\partial}{\partial\beta}\right],$$

(28)

and expressions for derivatives of the associated Legendre functions given in the Appendix. Finally, the stress field is obtained from the Hooke's law

$$\boldsymbol{\sigma} = \frac{E}{1+\nu}\left(\boldsymbol{\varepsilon} + \frac{\nu}{1-2\nu}\,\mathrm{tr}\,\boldsymbol{\varepsilon}\,\mathbf{I}\right),$$

(29)

where E and ν are the Young's modulus and Poisson ratio of the isotropic matrix and $\mathbf{I}$ is the second-rank unit tensor.

The Cartesian components of the stress tensor $\boldsymbol{\sigma}$ can be easily expressed via cylindrical components

$$\sigma_{xx} = \sigma_{rr}\cos^2\varphi + \sigma_{\varphi\varphi}\sin^2\varphi - 2\sigma_{r\varphi}\sin\varphi\cos\varphi,$$
$$\sigma_{yy} = \sigma_{rr}\sin^2\varphi + \sigma_{\varphi\varphi}\cos^2\varphi - 2\sigma_{r\varphi}\sin\varphi\cos\varphi,$$
$$\sigma_{xy} = \sigma_{r\varphi}\left(\cos^2\varphi - \sin^2\varphi\right) + \left(\sigma_{rr} - \sigma_{\varphi\varphi}\right)\sin\varphi\cos\varphi,$$
$$\sigma_{xz} = \sigma_{zr}\cos\varphi - \sigma_{z\varphi}\sin\varphi,$$
$$\sigma_{yz} = \sigma_{zr}\sin\varphi - \sigma_{z\varphi}\cos\varphi.$$

(30)

The traction vector at the torus surface $\alpha = \alpha_0$ is $\boldsymbol{t} = -\boldsymbol{e}_\alpha \cdot \boldsymbol{\sigma}$ with the outer unit normal

$$\boldsymbol{n} = \frac{1}{\cosh\alpha_0 - \cos\beta}\left\{(\cosh\alpha_0\cos\beta - 1)\,\cos\varphi, (\cosh\alpha_0\cos\beta - 1)\,\sin\varphi, \sinh\alpha_0\sin\beta\right\},$$

(31)

The principal moment produced by torus surface tractions is

$$\mathbf{M} = \int_s \boldsymbol{t} \times \boldsymbol{x}\; dA$$

(32)

where

$$\boldsymbol{x} = \frac{c}{\cosh\alpha_0 - \cos\beta}\left\{\sinh\alpha_0\,\cos\varphi, \sinh\alpha_0\,\sin\varphi, \sin\beta\right\}$$

(33)

is the position-vector of a point on the torus surface. The infinitesimal element of torus surface is given as [31]
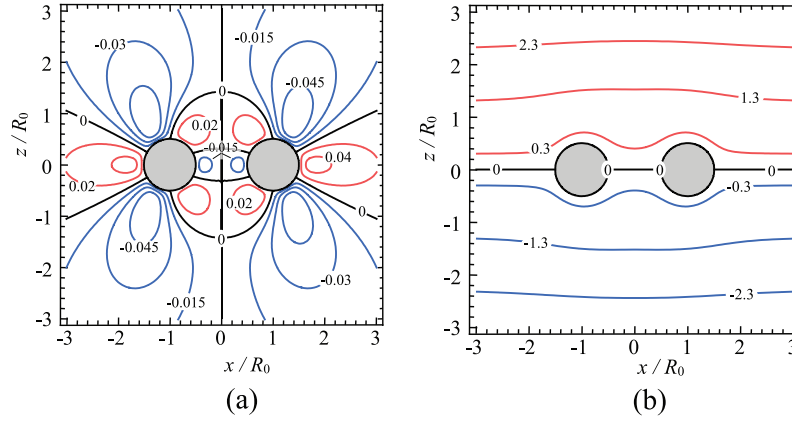
Figure 3. The distribution of the (a) $u_x = u_y$ and (b) u_z displacement components near rigid toroidal inhomogeneity ($R_0/r_0 = 2$) in infinite media under tension along the z-axis, i.e. for $\varepsilon_{zz}^\infty = 1$ and $\varepsilon_{yy}^\infty = \gamma_{yz}^\infty = 0$. The maps are plotted for a meridian plane $y = 0$. The displacement values are given in units of R_0 for $\nu = 0.3$.

$$dA = \frac{c^2 \sinh \alpha_0}{(\cosh \alpha_0 - \cos \beta)^2} \, d\varphi d\beta. \tag{34}$$

The solution obtained of the boundary value problem for an elastic medium with rigid torus is specified below for three load cases: ε_{zz}^∞, ε_{yy}^∞ and ε_{yz}^∞.

(i) Tension along z-axis. The nonzero component of remote elastic strain is ε_{zz}^∞. In this case the total displacement field has axial symmetry about the z-axis and vanishes on the surface of the torus. The maps for the displacement components u_y and u_z are shown in Figure 3 for the meridional cross-section of the matrix near the inhomogeneity.

The distribution of Cartesian component of stress vector on the torus surface ($\alpha = \alpha_0$) is shown in Figure 4.

(ii) Tension along y-axis. The nonzero component of remote elastic strain is ε_{yy}^∞. The total displacement vanishes on the surface of the rigid toroidal inclusion. The distribution of the displacement components u_y and u_z is illustrated in Figure 5 for the meridional cross-section of the matrix near the inhomogeneity. The distribution of Cartesian component of stress vector on the torus surface ($\alpha = \alpha_0$) is shown in Figure 6. It is seen that the boundary condition are satisfied on rigid torus surface for both (i) and (ii) load cases.

(iii) Simple shear in yz plane. The nonzero component of remote elastic strain is ε_{yz}^∞. Under shear, the toroidal inhomogeneity has rigid rotation on angle ω to be determined from the moment equilibrium condition with respect to the inhomogeneity

$$\mathbf{M}_\omega + \mathbf{M}_\gamma = 0 \tag{35}$$

where $\mathbf{M}_\omega$ is resultant moment required to produce rotation on angle ω and $\mathbf{M}_\gamma$ is the reactive moment caused by simple shear ε_{yz}^∞. Moments could be calculated using the equation (32)

$$\mathbf{M}_\omega = \int_S \boldsymbol{t}(\varepsilon_{yz}^\infty = 0) \times \boldsymbol{x} \; dA$$

$$\mathbf{M}_\gamma = \int_S \boldsymbol{t}(\omega = 0) \times \boldsymbol{x} \; dA \tag{36}$$
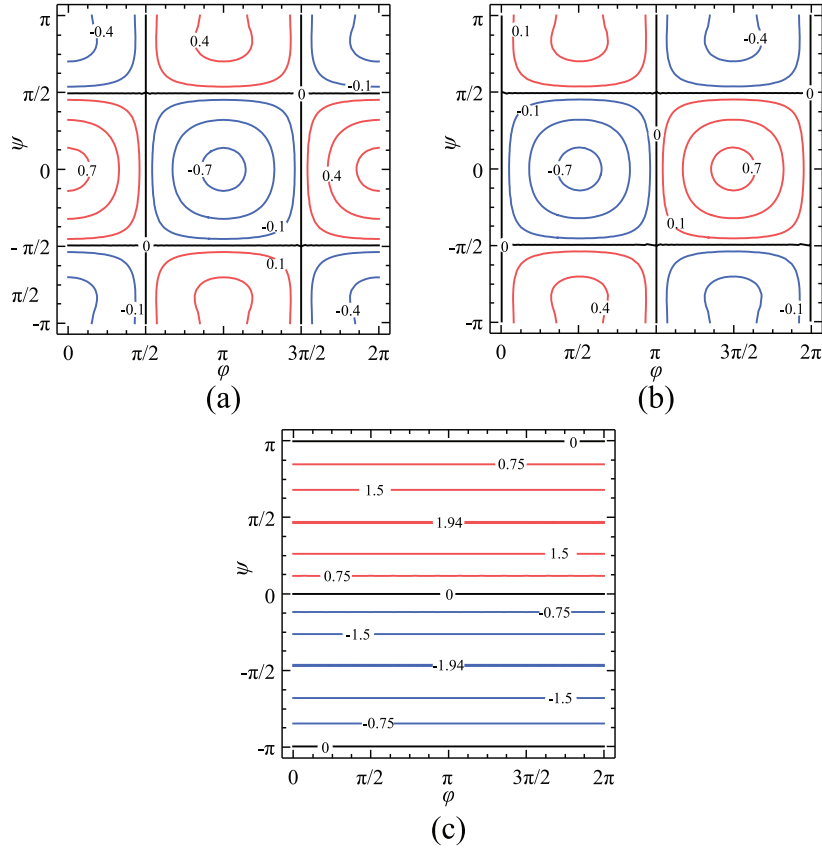
Figure 4. The distribution of the (a) t_x, (b) t_y, and (c) t_z traction components at the torus surface $\alpha = \alpha_0$, $R_0/r_0 = 2$ with respect to azimuth φ and poloidal angel ψ. The nonzero component of remote strain is $\varepsilon_{zz}^\infty = 1$. The stress values are given in units of E for $\nu = 0.3$.

Due to the linearity of the problem, forces and moments are proportional to the displacements and rotations, respectively. Then, accounting for the equilibrium equation (34), the rotation angle can be calculated as

$$\omega = 2 \left| \frac{\mathbf{M}_\gamma}{\mathbf{M}_\omega} \right| \varepsilon_{yz}^\infty \tag{37}$$

The dependence of ω on the aspect ratio of torus is shown in Figure 7.

The distribution of the displacement components u_y and u_z under simple shear ε_{yz}^∞ is shown in Figure 8 for the meridional cross-section of the matrix near the torus.

The distribution of Cartesian component of the traction vector on torus surface is shown in Figure 9. We now can calculate the components of the stiffness contribution tensor $\mathbf{N}$ for a rigid toroidal inhomogeneity using equations (1) and (2), namely

$$\mathbf{N} : \boldsymbol{\varepsilon}^\infty = \frac{1}{V^*} \int_S \boldsymbol{t}\boldsymbol{x} \, dA, \tag{38}$$

where $V^* = 2\pi^2 r_0^2 R_0$ is the volume of the torus and dA is the infinitesimal element of torus surface (see equation (34)). In the toroidal coordinate system traction $\boldsymbol{t}$ and position vector $\boldsymbol{x}$ is given by equations (29)–(31) and (34). Then the normalized dependence of the stiffness contribution tensor $\boldsymbol{N}$ on torus aspect ratio $\lambda = r_0/R_0$ can be obtained from equation (38).
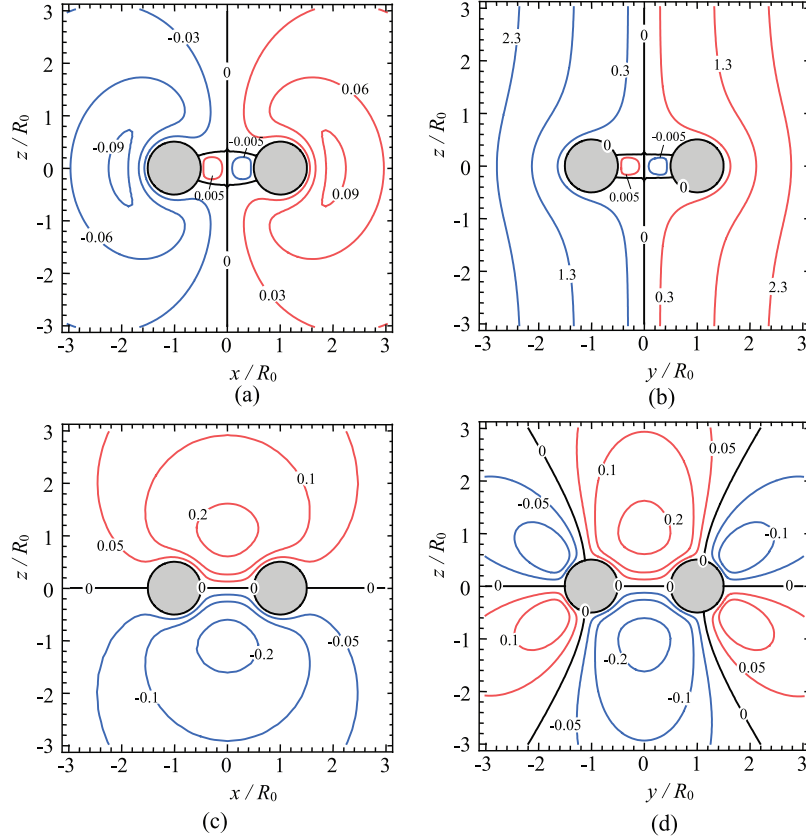
Figure 5. The distribution of the (a) u_x, (b) u_y, and (c, d) u_z displacement components near rigid toroidal inhomogeneity ($R_0/r_0 = 2$) in infinite media under tension along the y-axis, i.e. for $\varepsilon_{yy}^\infty = 1$ and $\varepsilon_{zz}^\infty = \gamma_{yz}^\infty = 0$. The maps are plotted for the meridian planes: (a) and (c) for $y = 0$; (b) and (d) for $x = 0$. The displacement values are given in units of R_0 for $\nu = 0.3$.

4. Finite element model

To verify the analytical solution, we also calculate components of the stiffness contribution tensors using finite element analysis (FEA). To produce the necessary 3D mesh of the considered shape we start by generating surface mesh in a custom MATLAB script [36,37]. A torus surface is defined parametrically using equation (6). Since the coordinates are stored in the form of an ordered list they can easily be connected into the continuous mesh with triangular elements. Note that each mesh generated using our script is composed of approximately 30,000 surface elements (see Figure 10).

Torus surface mesh is then placed into a large reference volume V that has cubic shape with sides at least five times bigger than the largest linear dimension of the inhomogeneity to reduce boundary effects and simulate remote loading. This setup is auto meshed with non-linear tetrahedral 3D elements due to higher accuracy of results compared to linear elements. An example of the mesh is given in Figure 11. To simulate perfectly rigid inhomogeneity we assume that the ratio of matrix and inhomogeneity Young's moduli is $E_i/E = 10^{10}$. The boundary ∂V of the reference volume I is subject to the kinematic conditions

$$\boldsymbol{u}|_{\partial V} = \boldsymbol{\varepsilon}^\infty \cdot \boldsymbol{x} \qquad (39)$$

At the next step, to find all nonzero components of tensor **N** we perform a set of six load cases in FEA package MSC Marc Mentat: three normal loadings in the directions of three global coordinate axes and three shear loads according to equation (39). Once the numerical simulations are completed for the given shape, the result files are processed to calculate all volume-averaged stress components within V from each load case:
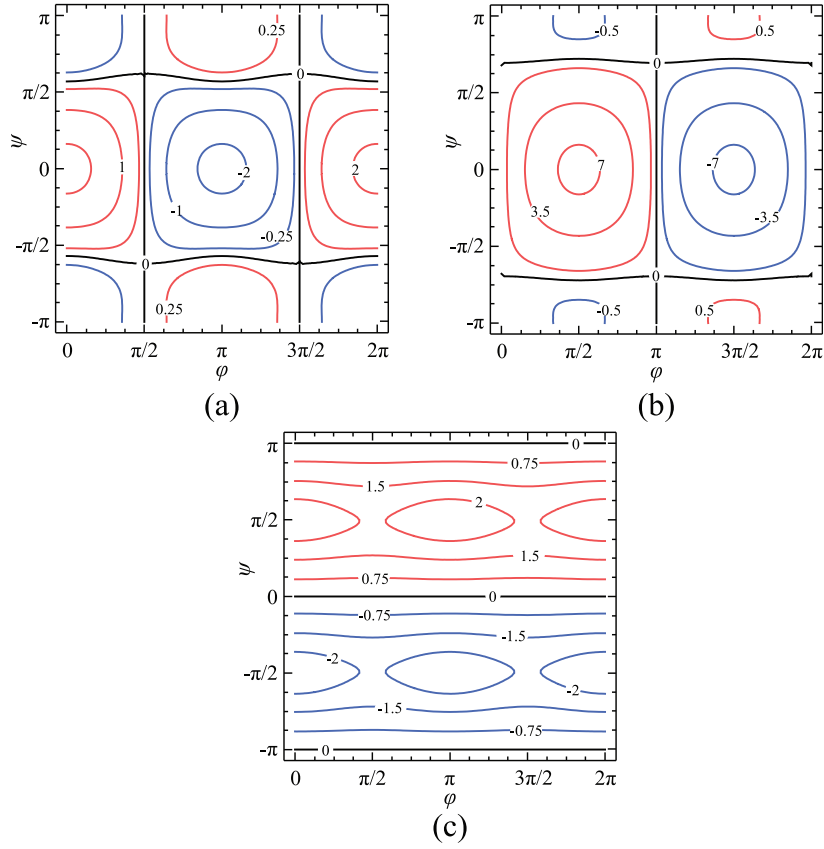
Figure 6. The distribution of the (a) t_x, (b) t_y and (c) t_z traction components at the torus surface $\alpha = \alpha_0$, $R_0/r_0 = 2$ with respect to azimuth φ and poloidal angel ψ. The nonzero component of remote strain is $\varepsilon_{yy}^{\infty} = 1$. The stress values are given in units of E for $\nu = 0.3$.
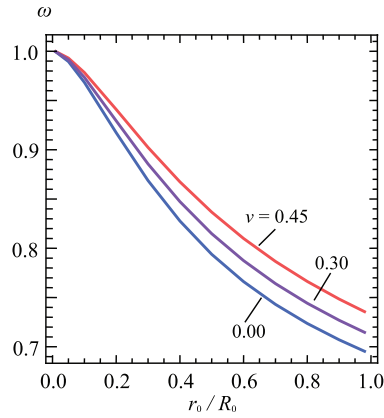

Figure 7. Dependences of rotation angle ω of inclusion with respect to torus aspect ratio r_0/R_0 for $\gamma_{yz}^{\infty} = 1$ and different values of Poisson ratio $0.00, 0.30$, and 0.45.

$$\left\langle \sigma_{ij} \right\rangle_m = \frac{1}{V} \sum_{l=1}^{Ne} (\sigma_{ij}^{(l)})_m V^{(l)} (i,j = 1, 2, 3; m = 1, 2, ..., 6) \tag{40}$$

where $\left\langle \sigma_{ij} \right\rangle_m$ is the volume average of the stress component ij calculated from the mth load case, V is the reference volume, $(\sigma_{ij}^{(l)})_m$ is the stress component ij at the centroid of the finite element l calculated
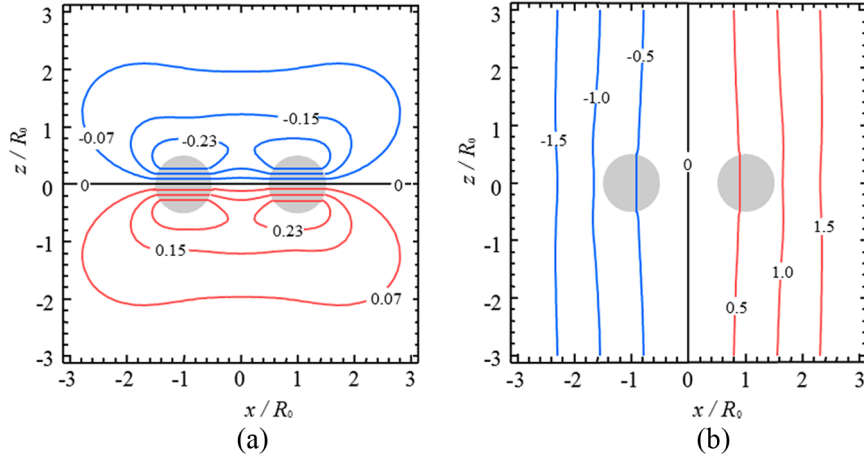
Figure 8. The distribution of the (a) u_y and (b) u_z displacement components near rigid toroidal inhomogeneity ($R_0/r_0 = 2$) in infinite media under simple shear in the yz plane, i.e. for $\gamma_{yz}^\infty = 1$, $\omega \approx 0.794$, and $\varepsilon_{yy}^\infty = \varepsilon_{zz}^\infty = 0$. The maps are plotted for the meridian plane $x = 0$. The displacement values are given in units of R_0 for $\nu = 0.3$.
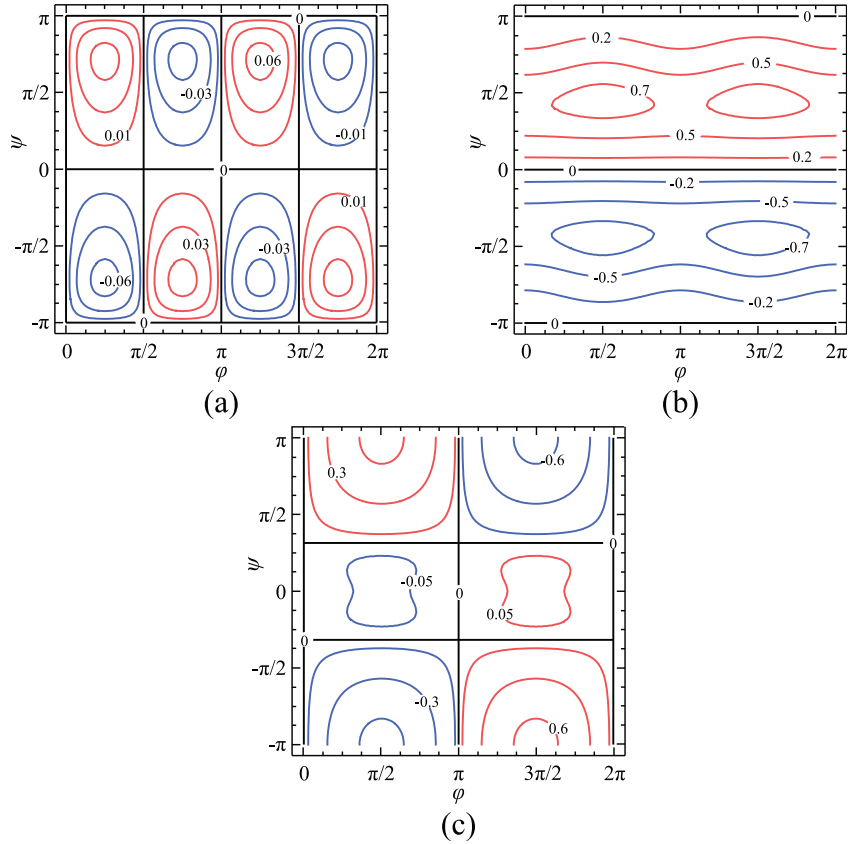

Figure 9. The distribution of the (a) t_x, (b) t_y, and (c) t_z traction components at the torus surface $\alpha = \alpha_0$, $R_0/r_0 = 2$ with respect to azimuth φ and poloidal angel ψ. The nonzero component of remote strain is $\gamma_{yz}^\infty = 1$. The stress values are given in units of E for $\nu = 0.3$.

from the mth load case, $V^{(l)}$ is the volume of the element l, and N_e is the total number of elements in the model.
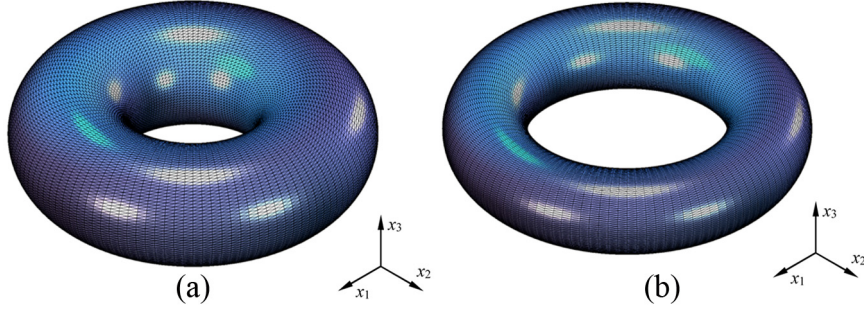
Figure 10. Torus surface meshes for different ratio r_0/R_0 (a) 0.5 and (b) 0.3.
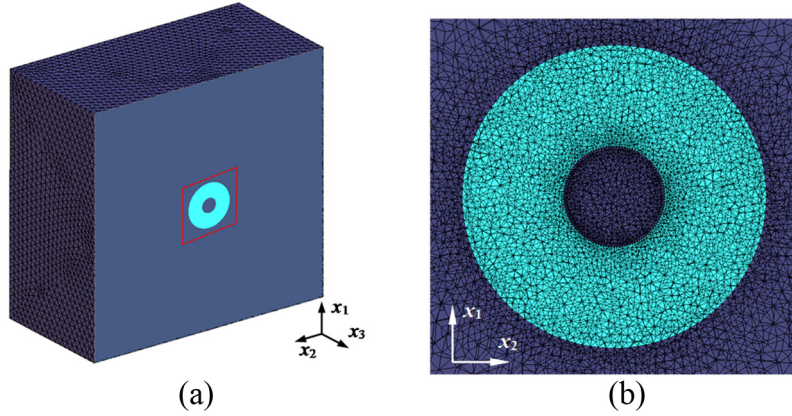

Figure 11. Example of a mesh density of the matrix and torus with $r_0/R_0 = 0.5$: (a) general view; (b) close-up view of the highlighted region.

Given the average stress components we then calculate the stiffness contribution tensor from:

$$N_{ijkl}(\varepsilon^{\infty}_{kl})_m = \langle \sigma_{ij} \rangle_m - (\sigma^{\infty})_m (\text{summation over } k, l = 1, 2, 3) \qquad (41)$$

where $(\varepsilon^{\infty}_{kl})_m$ are the components of the prescribed strain and $(\sigma^{\infty}_{ij})_m$ are the stress components inside V in the absence of the inhomogeneity. Components of the stiffness contribution tensors are than normalized by particle volume fraction and matrix Young's modulus E as follows, $\bar{N}_{ijkl} = \frac{V}{EV^*} N_{ijkl}$, where V^* is torus inhomogeneity volume. Figure 12 illustrates comparison of the nonzero components of stiffness contribution tensor calculated analytically using equation (38) with ones obtained by FEA.

5. Approximation by spheroid

We now compare the obtained results with ones for stiffness contribution tensor of an oblate rigid spheroid of the aspect ratio χ components of this tensor can be written as follows:

$$N_{1111} = \frac{p_6}{4(p_1 p_6 - p_3^2)} + \frac{1}{2p_2}, \quad N_{1122} = \frac{p_6}{4(p_1 p_6 - p_3^2)} - \frac{1}{2p_2}, \quad N_{1212} = \frac{1}{2p_2}, \quad N_{3333} = \frac{p_6}{p_1 p_6 - p_3^2};$$

$$N_{1133} = -\frac{p_3}{2(p_1 p_6 - p_3^2)}, \qquad N_{1313} = \frac{1}{p_5},$$
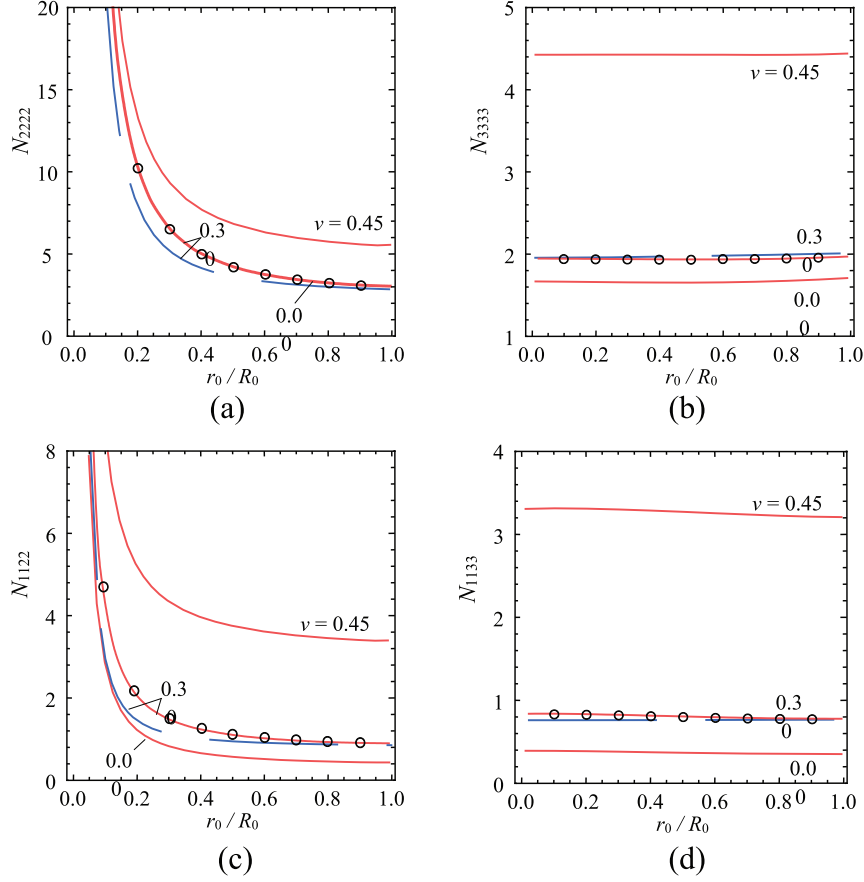
where

Figure 12. Normalized nonzero components of the stiffness contribution tensor of inhomogeneity (a) $N_{1111} = N_{2222}$, (b) N_{3333}, (c) N_{1122}, (d) N_{1133}, (e) N_{1212}, and (f) $N_{1313} = N_{2323}$ as function of the aspect ratio r_0/R_0. The solid curves correspond to the rigid toroidal inclusion; The dashed curves correspond to the rigid ellipsoidal inclusion; the FEM results are noted by marks. The stiffness values are given in units of $\varepsilon_{ij}E$ for different values of Poisson ratio 0.0, 0.3, and 0.45.

$$p_1 = \frac{1}{2\mu}[(1-\kappa)f_0 + \kappa f_1]; \quad p_2 = \frac{1}{2\mu}[(2-\kappa)f_0 + \kappa f_1], \qquad p_3 = p_4 = -\frac{\kappa f_1}{\mu},$$

$$p_5 = \frac{1}{\mu}[1 - f_0 - 4\kappa f_1], \qquad p_6 = \frac{1}{\mu}[(1-\kappa)(1-2f_0) + 2\kappa f_1].$$

(42)

and the following notation is used:

$$\mu = \frac{E}{2(1+\nu)}, \kappa = \frac{1}{2(1-\nu)}, f_0 = \frac{\chi^2(1-g)}{2(\chi^2-1)}, f_1 = \frac{\chi^2}{4(\chi^2-1)}[(2\chi^2+1)g - 3],$$

$$g = \begin{cases} \dfrac{1}{\chi\sqrt{1-\chi^2}}\arctan\dfrac{\sqrt{1-\chi^2}}{\chi}, & \text{oblate shape } (\chi<1) \\[3mm] \dfrac{1}{2\chi\sqrt{\chi^2-1}}\ln\dfrac{\chi+\sqrt{\chi^2-1}}{\chi-\sqrt{\chi^2-1}}, & \text{prolate shape } (\chi>1) \end{cases}$$

(43)

Argatov and Sevostianov [23], using asymptotic methods, showed that in-plane components of the stiffness contribution tensor of a thin rigid torus can be approximated with good accuracy by the corresponding components calculated for a rigid spheroid that has the same radius and the same volume. For an oblate spheroid, it gives the aspect ratio of the spheroid in terms of the aspect ratio of the torus $\lambda = r_0/R_0$ as follows:

$$\chi = \frac{3\pi\lambda^2}{2\,(1+\lambda)^3}.$$ (44)

Equation (44) gives us a spheroid that has the same volume and the same radius as the torus. These components are shown in Figure 12(a), (c), and (e) as functions of λ.

Out-of-plane components of the stiffness contribution tensor of a rigid torus can be approximated by the in-plane components of a rigid prolate spheroid that has the same radius and the same volume. In this case, to preserve the radius and the volume, the aspect ratio of the spheroid has to be

$$\chi = \frac{3\pi}{2\lambda}$$ (55)

Figure 12(b), (d), and (f) illustrate a comparison between the components of the stiffness contribution tensors for rigid inhomogeneities of toroidal and prolate spheroidal pores. It is seen that the lines are quite close to each other with the exception of N_{1313}.

6. Discussion and conclusions

We solved an elasticity boundary-value problem for an infinite elastic medium containing a rigid toroidal inhomogeneity subjected to remotely applied uniform strains. The solution is obtained in explicit form of associated Legendre function's series using the approach proposed by Eroshkin and Tsukrov [27]. Displacement and traction is determined as a function of coordinates, torus parameters and strain components applied at infinity. We managed to combine the procedures for solving the axisymmetric ($k = 0$) and asymmetric ($k \geq 1$) case and write the solution in the most general form. The boundary-value problems were reduced to infinite systems of algebraic equations with three-diagonal matrices. We succeeded in extending the classical method of solving finite algebraic equations with a tridiagonal matrix to the case of an infinite number of equations.

Considering the toroidal inhomogeneity subject to simple shear in the meridional plane, we have taken into account the rigid rotation of the inhomogeneity. The angle of rotation can be calculated from the equation of moment equilibrium. The angle decreases when the torus aspect ratio increases.

The obtained solution is used to get explicit expressions for the components of stiffness contribution tensor of the rigid toroidal inhomogeneity. The results are verified by comparison with finite element simulating. The components of the stiffness contribution tensor for a torus are compared with ones for a rigid spheroid having the same radius and the same volume as torus. It is shown that the components of the stiffness contribution tensor for an oblate spheroid serve as good approximations for corresponding in-plane components of the torus while two out-plane components can be approximated by components of the stiffness contribution tensor for a prolate spheroid.

The expression for stiffness contribution tensor yields the possibility to calculate effective elastic properties of a material containing multiple toroidal inhomogeneities. Indeed, if interaction between the inhomogeneities is neglected, each inhomogeneity can be assumed to be subjected to the same remotely applied strain, their contributions into the change in the stiffness tensor can be treated separately. In none interaction approximation the extra stiffness due to inhomogeneities of the same shape can always be represented in the form

$$\Delta \mathbf{C} = \frac{1}{V}\sum_i V_i \mathbf{N}^{(i)}$$ (56)

where summation over inhomogeneities may be replaced by integration over their orientation. The non-interaction approximation, in turn, serves as the basic building block for various homogenization schemes – self-consistent, differential, Mori–Tanaka, Maxwell, etc. [38].

References

[1] Bogicevic, C, Thorner, G, Karolak, F, et al. Morphogenesis mechanisms in the solvothermal synthesis of $BaTiO_3$ from titanate nanorods and nanotubes. *Nanoscale* 2013; 7: 3594–3603.

[2] Horstmann, B, Gallant, B, Mitchell, R, et al. Rate-dependent morphology of Li_2O_2 growth in Li–O_2 batteries. *J Phys Chem Lett* 2013; 4: 4217–4222.

[3] Chen, Y, Freunberger, SA, Peng, Z, et al. Charging a Li–O_2 battery using a redox mediator. *Nat Chem* 2013; 5: 489–494.

[4] Alexander, L, Dhaliwal, K, Simpson, J, et al. Dunking doughnuts into cells—selective cellular translocation and in vivo analysis of polymeric micro-doughnuts. *Chem Commun* 2008: 3507–3509.

[5] Xia, F, Liu, J, Gu, D, et al. Microwave absorption enhancement and electron microscopy characterization of $BaTiO_3$ nano-torus. *Nanoscale* 2011; 3: 3860–3867.

[6] Onaka, S, Sato, H, and Kato, M. Elastic states of doughnut-like inclusions with uniform eigenstrains treated by averaged Eshelby tensors. *Philos Mag Lett* 2002; 82: 1–7.

[7] Palanisamy, A, and Guo, Q. Giant tubular and toroidal vesicles from self-assembled triblock copolymer–polyaniline complexes in water. *Chem Commun* 2015: 11100–11103.

[8] Haridas, V, Sapala, AR, and Jasinski, JP. Self-assembling triazolophanes: from croissants through donuts to spherical vesicles. *Chem Commun* 2015; 6905–6908.

[9] Park, CH, Chung, N, and Lee, J. Monodisperse red blood cell-like particles via consolidation of charged droplets. *J Colloid Interface Sci* 2011; 361: 423–428.

[10] Zimmerman, RW. Compressibility of two-dimensional cavities of various shapes. *J Appl Mech* 1986; 53: 500–504.

[11] Kachanov, M, Tsukrov, I, and Shafiro, B. Effective moduli of solids with cavities of various shapes. *Appl Mech Rev* 1994; 47: S151–S174.

[12] Tsukrov, I, and Novak, J. Effective elastic properties of solids with defects of irregular shapes. *Int J Solids Struct* 2002; 39: 1539–1555.

[13] Tsukrov, I, and Novak, J. Effective elastic properties of solids with two-dimensional inclusions of irregular shapes. *Int J Solids Struct* 2004; 41: 6905–6924.

[14] Fabrikant, VI. *Applications of potential theory in mechanics: a selection of new results*. Dordrecht, the Netherlands: Kluwer Academic Publishers, 1989.

[15] Sevostianov, I, and Kachanov, M. On elastic compliances of irregularly shaped cracks. *Int J Fract* 2002; 114: 245–257.

[16] Grechka, V, Vasconcelos, I, and Kachanov, M. The influence of crack shape on the effective elasticity of fractured rocks. *Geophysics* 2006; 71: D153–D160.

[17] Mear, ME, Sevostianov, I, and Kachanov, M. Elastic compliances of non-flat cracks. *Int J Solids Struct* 2007; 44: 6412–6427.

[18] Kachanov, M, and Sevostianov, I. Rice's Internal variables formalism and its implications for the elastic and conductive properties of cracked materials, and for the attempts to relate strength to stiffness. *J Appl Mech* 2012; 79: 031002.

[19] Sevostianov, I, Kachanov, M, and Zohdi, T. On computation of the compliance and stiffness contribution tensors of non ellipsoidal inhomogeneities. *Int J Solids Struct* 2008; 45: 4375–4383.

[20] Sevostianov, I, and Giraud, A. On the compliance contribution tensor for a concave superspherical pore. *Int J Fract* 2012; 177: 199–206.

[21] Chen, F, Sevostianov, I, Giraud, A, et al. Evaluation of the effective elastic and conductive properties of a material containing concave pores. *Int J Eng Sci* 2015; 97: 60–68.

[22] Sevostianov, I, Chen, F, Giraud, A, et al. Compliance and resistivity contribution tensors of axisymmetric concave pores. *Int J Eng Sci* 2016; 101: 14–28.

[23] Argatov, I, and Sevostianov, I. Rigid toroidal inhomogeneity in an elastic medium. *Int J Eng Sci* 2011; 49: 61–74.

[24] Onaka, S, Kobayashi, N, Fujii, T, et al. Energy analysis with a superspherical shape approximation on the spherical to cubical shape transitions of coherent precipitates in cubic materials. *Mater Sci Eng A* 2003; 347: 42–49.

[25] Onaka, S. Strain fields caused by doughnut-like and tubular inclusions with uniform eigenstrains. *Mech Res Commun* 2005; 32: 316–322.

[26] Radi, E, and Sevostianov, I. Toroidal insulating inhomogeneity in an infinite space and related problems. *Proc R Soc Lond A* 2016; 472: 20150781.

[27] Eroshkin, O, and Tsukrov, I. On micromechanical modeling of particulate composites with inclusions of various shapes. *Int J Solids Struct* 2005; 42: 409–427.

[28] Solovie, v YI. The axisymmetric problem of elasticity for a torus and a space with toroidal cave. *Mekh Tverd Tela* 1969: 99–105.

[29] Podil'chuk, YN, and Kirilyuk, VS. Nonaxially symmetric deformation of a torus. *Sov Appl Mech* 1983; 119: 743–748.

[30] Kirilyuk, VS. Stress concentration in an isotropic medium with an elastic toroidal inhomogeneity. *Sov Appl Mech* 1988; 24: 11–14.

[31] Morse, PM, and Feshback, H. *Methods of theoretical physics*. New York: McGraw-Hill, 1953.

[32] Lebedev, NN, and Silverman, RA. *Special functions & their applications*. Upper Saddle River, NJ: Prentice-Hall, 1965.

[33] Hobson, EW. *Spherical and ellipsoidal harmonics*. Cambridge: Cambridge University Press., 1931.
[34] Bateman, H, and Erdelyi, A. *Higher transcendental functions*. New York: McGraw-Hill, 1953.
[35] Krokhmal, PA. Exact solution of the displacement boundary-value problem of elasticity for a torus. *J Eng Math* 2002; 44: 345–368.
[36] Trofimov, A, Drach, B, Kachanov, M, et al. Effect of a partial contact between the crack faces on its contribution to overall material compliance and resistivity. *Int J Solids Struct*. Epub ahead of print 1 March 2017. DOI: 10.1016/j.ijsolstr.2016.12.028.
[37] Trofimov, A, Drach, B, and Sevostianov, I. Effective elastic properties of composites with particles of polyhedral shapes. *Int J Solids Struct* 2017; 120: 157–170.
[38] Sevostianov, I, and Kachanov, M. Non-interaction approximation in the problem of effective properties. In: Kachanov, M, and Sevostianov, I (eds.) *Effective properties of heterogeneous materials*, Springer Science & Business Media, 2013, 1–95.

Appendix

Legendre functions

The following recursive relations hold for the function $P_{n-1/2}^k$:

$$P_{n-1/2}^1(\cosh\alpha) = \frac{n+1/2}{\sinh\alpha}\left[P_{n+1/2}(\cosh\alpha) - \cosh\alpha\, P_{n-1/2}(\cosh\alpha)\right],$$

$$P_{n-1/2}^2(\cosh\alpha) = (n^2 - 1/4)\, P_{n-1/2}(\cosh\alpha) - 2\coth\alpha\, P_{n-1/2}^1(\cosh\alpha),$$

$$P_{n-1/2}^3(\cosh\alpha) = (n^2 - 9/4)\, P_{n-1/2}^1(\cosh\alpha) - 4\coth\alpha\, P_{n-1/2}^2(\cosh\alpha).$$

By using the recursive properties of Legendre functions [35] one may obtain

$$\frac{d}{d\alpha}P_{n-1/2}(\cosh\alpha) = \frac{1+2n}{2\,\sinh\alpha_0}\left[P_{n+1/2}(\cosh\alpha) - \cosh\alpha\, P_{n-1/2}(\cosh\alpha)\right], ()$$

$$\frac{d}{d\alpha}P_{n-1/2}^k(\cosh\alpha) = \left[n^2 - \left(k - \frac{1}{2}\right)^2\right]P_{n-1/2}^{k-1}(\cosh\alpha) - k\coth\alpha\, P_{n-1/2}^k(\cosh\alpha), (k \geq 1)$$

and similar relations hold for $Q_{n-1/2}$.

The following useful definite integrals involving the Legendre functions and associate Legendre functions of first and second kind, denoted as $P_{n-1/2}^k$ and $Q_{n-1/2}^k$, respectively, have been used in the present work:

$$\int_{-\pi}^{\pi}\frac{\sin\beta\,\sin n\beta\,d\beta}{(\cosh\alpha - \cos\beta)^{3/2}} = \frac{4\sqrt{2}}{n}\,Q_{n-1/2}(\cosh a), \tag{A1}$$

$$\int_{-\pi}^{\pi}\frac{\cos n\beta\,d\beta}{(\cosh\alpha - \cos\beta)^{3/2}} = \frac{4\sqrt{2}}{\sinh\alpha}\,Q_{n-1/2}^1(\cosh a), \tag{A2}$$